

Genesis of the *terrae rossae* of the Sierra Gádor (Andalusia, Spain)

R. DELGADO^a, J. M. MARTÍN-GARCÍA^b, C. OYONARTE^c & G. DELGADO^a

^aDepartamento de Edafología y Química Agrícola, Facultad de Farmacia, Universidad de Granada, 18071 Granada, ^bDepartamento de Geología, Facultad de Ciencias Experimentales, Universidad de Jaén, 23071 Jaén, and ^cDepartamento de Edafología y Química Agrícola, Escuela Politécnica Superior, Universidad de Almería, 04120 Almería, Spain

Summary

Some aspects of the genesis of *terrae rossae* are still subject to controversy while others related to the genesis of the mineral fraction have been studied very little. We have studied four *terrae rossae* over limestone (two Chromic-Leptic Luvisols, a Rhodi-Leptic Luvisol and a Chromi-Leptic Cambisol) in Sierra Gádor (Almería, southern Spain), in particular the various formation processes by (i) examination of their morphological, analytical and mineralogical characteristics (including crystallochemical parameters of the mica), (ii) examination of the insoluble residue of the gravel and rock, (iii) scanning electron microscopy (SEM) of sand and silt grains, and (iv) examination of the geochemistry of the soil solution. We have investigated the autochthonous or allochthonous nature of the soil material (fine earth and gravel) in relation to the rocky substrate, concluding that both origins are possible. Our SEM study of the morphology of the quartz grains shows that some are insoluble residue and some are probably wind blown from desert and coastal sources. The micas in the fine earth fractions are inherited from the insoluble residue. Comparison of the crystallochemical parameters of micas in the insoluble residue and the soil clay shows that the clay has more Si^{IV} and (Fe, Mg)^{VI}, and less Al^{IV}, Al^{VI} and x (layer charge) than the insoluble residue. It also has fewer polytypes $2M_1$ and more $1M$ and has a smaller crystal size, especially in B horizons. The kaolinite is of varied origins including neoformation and inheritance from underlying rock. Some of the kaolinite and some mica has been blown in from elsewhere, probably from desert and coastal sources. The soils have undergone other typical processes of *terrae rossae* including dissolution of carbonate, illuviation of clay and iron oxides, and rubifaction.

Introduction

Terrae rossae are common in Mediterranean climates and over limestone. Aspects of the genesis of these reddish, clayey mineral soils with disrupted horizons are still controversial. According to the 'residual theory' (Bronger & Bruhn-Lobin, 1997), the fine material of the soil is autochthonous and derived from the dissolution of carbonate and accumulation of insoluble residue *in situ* (Moresi & Mongelli, 1988). Other workers suggest an allochthonous origin; for example, Olson *et al.* (1980) show that the considerable thickness of the red clayey material overlying limestones in Indiana, USA, could be best explained by a combination of pedological and geomorphological processes other than simple accumulation of insoluble limestone residue. The possibility of contributions of wind-blown material is reviewed by Yaalon (1997) who

considers that almost all soils in the Mediterranean region contain some Saharan aeolian dust, which may account for up to 50% of the fine earth.

The various processes that could affect the mineral fractions of *terrae rossae* are as follows.

- 1 Weathering of primary minerals including carbonate dissolution.
- 2 Inheritance of micaceous minerals. Nobody has studied crystallochemistry of the latter process in *terrae rossae* although Martín-García *et al.* (1997, 1998) have studied this process in other red soils.
- 3 Transformation of phyllosilicate minerals such as micas into smectites, vermiculites and interstratified phases. Other origins are also possible for these phases including inheritance or neoformation.
- 4 Neoformation of kaolinite which increases with soil evolution. Kaolinite in *terrae rossae* could, however, be inherited from the parent material or even transformed from other minerals.

Correspondence: R. Delgado. E-mail: rdelgado@ugr.es

Received 15 March 2001; revised version accepted 26 September 2002

5 Enrichment in sesquioxides (principally iron oxides) which give the soil a red colour. The concentration of iron oxides in the form of haematites in soil increases the degree of redness, eventually reaching saturation (Torrent *et al.*, 1983).

6 Illuviation of clays and iron oxides.

Some earlier investigations compared the insoluble residue of the parent rock with the fine earth of the soil. Another technique occasionally used in genetic studies of *terrae rossae* is the study of mineral grains, often quartz, by SEM (Flageollet, 1981).

Terrae rossae are common in Spain but there has been little research on such soils in the mountains of southern Spain. We have studied the various formation processes of *terrae rossae* from Sierra Gádor in Andalusia. Special attention has been

paid to the origin of micas (not previously known in these soils) and the genesis of kaolinite and quartz.

The soils

Four profiles representative of the *terrae rossae* in southeastern Spain (Sierra Gádor mountain range) close to the Mediterranean sea (Table 1, Figure 1) were sampled. The parent rocks are compact Triassic limestones (Table 1) that form a mountainous karst landscape in which *terrae rossae* cover 10% of the ground. Man's influence is widespread, including (i) 19th-century mining activity, (ii) deforestation, (iii) cultivation over a long period, but now largely abandoned, (iv) reafforestation, and (v) traditional migratory grazing. The sampling

Table 1 General characteristics of the profiles sampled

Profile	Soil classification ^a	Altitude /m	Slope /%	Vegetation and land use	Substratum	Soil climate				
						Water surplus /mm ^b	Water deficit /mm ^b	Precipitation /mm ^b	Moisture regime	Temperature regime
P1	Chromi-Leptic Luvisol	1500	18	Scrub (thymus) and abandoned crops	Limestone (marly)	288	333	608	Xeric	Mesic
P2	Rhodi-Leptic Luvisol	1600	27	Scrub and reforested pines	Dolomitic limestone	302	309	631	Xeric	Mesic
P3	Chromi-Leptic Luvisol	1100	3	Scrub and abandoned crops	Cemented limestone breccia	149	389	487	Xeric	Thermic
P4	Chromi-Leptic Cambisol	1650	38	Fescue association	Cemented limestone breccia	283	254	654	Xeric	Mesic

^aFAO (1998).

^bAnnual quantities, moderate hydric laminar erosion in all cases.

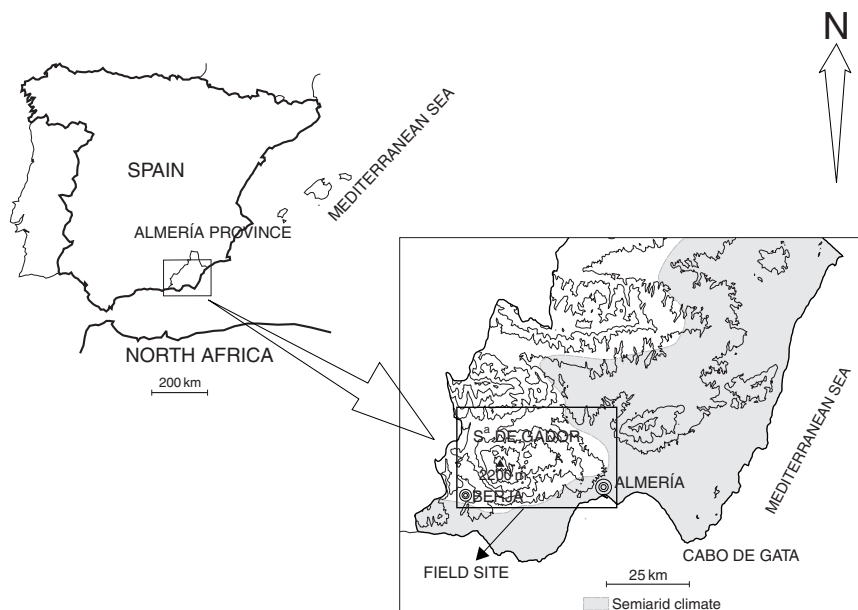


Figure 1 Sampling locality.

Table 2 Morphological characteristics of the profiles

Profile	Horizon notation	Depth /cm	Munsell colour (moist)	Structure ^a	Cutans ^b	Porosity ^c	Boundaries ^d
P1	A	0–8	5YR 3/3	gr, m, 1	–	vs, f–vf, 3	c, w
	Bt	8–32	2.5YR 3.5/4.5	sb, m, 2	il, ds, t	in, vf, 2	c, w
	2R	>32	–	–	–	–	–
P2	Ah	0–17	5YR 3/3	gr, m, 1/sb, m, 1	–	in, f, 3	g, w
	Bt	17–38/50	2.5YR 3/4	sb, m, 2	sp	in, f, 3	a, b
	R	>38/50	–	–	–	–	–
P3	A	0–16	5YR 3/4	gr, f, 2	–	in, vf, 3	c, s
	2Bt	16–43	2.5YR 3.5/4	sb, m, 2	sp, ct, t	in, vf, 2	c, w
	2R	>43	–	–	–	–	–
P4	Ah	0–17	5YR 3/3	gr, m, 2	–	in, f/vf, 3	c, s
	Bw	17–43	2.5YR 4/5	sb, m, 2	sp, ct, t	in, vf, 1	a, s
	C	43–57	7.5YR 5/6	ag, m, 2	–	in, 2	a, ir
	2R	>43/57	–	–	–	–	–

^aStructure. Shape: gr, granular; sb, subangular blocky; ag, angular blocky. Size: m, medium; f, fine. Grade: 1, strong; 2, moderate.

^bCutans. Type: il, illuviation cutan; sp, pressure face. Quantity: ds, discontinuous; ct, continuous. Thickness: t, thin.

^cPorosity. Type: vs, vesicles; in, interstitial. Size: f, fine; vf, very fine. Abundance: 1, few; 2, common; 3, many.

^dBoundaries of horizons. Distinctness: a, abrupt; c, clear; g, gradual. Topography: s, smooth; w, wavy; ir, irregular; b, broken.

areas have been variously affected by deforestation, cultivation and tree planting (Table 1).

The soils studied are Chromic-Leptic Luvisols (P1 and P3), a Rhodi-Leptic Luvisol (P2) and a Chromi-Leptic Cambisol (P4) (FAO, 1998) (Haploxeralfs and Haploxerept in *Soil Taxonomy*, Soil Survey Staff, 1999), with horizon sequences Ah(A)–Bt–BtR and Ah–Bw–C–R (Table 2). The soil moisture regime is xeric, with a marked excess of water in autumn/winter, alternating with long dry summers (Table 1, Figure 2). The present vegetation and the human history of the area suggest that these soils have been eroded, as can be seen from their thinness; all the profiles can be qualified as Leptic (Table 2) since they have continuous hard rock between 25 and 100 cm depth.

Methods

The morphology of each horizon (Table 2) was described in detail using the colours of the Munsell system. The micro-morphology of the Bt horizons was characterized in thin sections and some morphological characteristics of the gravel and parent rocks were described visually (Table 3).

Granulometric analysis was carried out by sieving and sedimentation (Robinson pipette) considering: clay (< 2 µm), silt (2–50 µm), fine sand (50–200 µm), coarse sand (200–2000 µm), and gravel (> 2 mm), fine gravel (2–8 mm) and coarse gravel (> 8 mm); these fractions were separated for later analysis. The insoluble residue of the gravel and rock was obtained by treatment with diluted 0.5 M HCl solution and subsequent dialysis, with the pH controlled >5. In the same process the

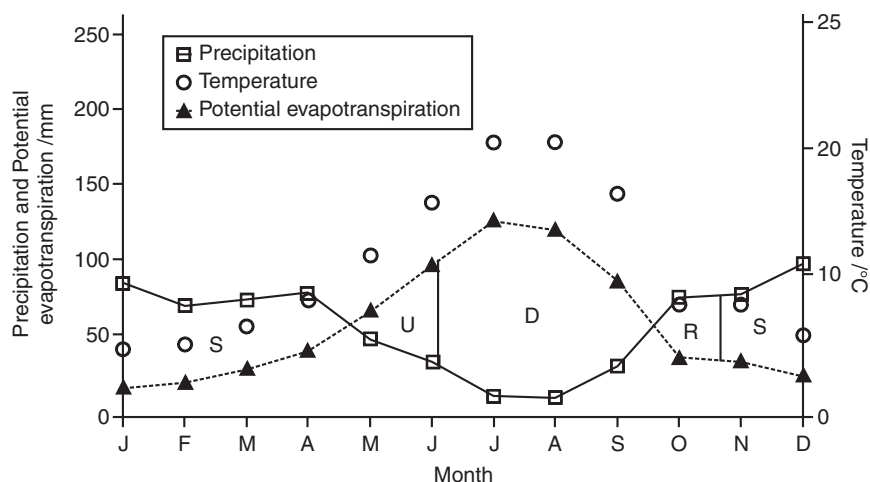


Figure 2 Climate and soil water balance of soil P2. S, surplus; U, utilization; D, deficit; R, recharge. Available water storage profile = 54 mm.

Table 3 Morphological, analytical and mineralogical characteristics of the gravels, rocks and insoluble residue (IR)

Profile	Horizon	Morphological characteristics ^a			Particle size distribution of insoluble residue					Rock and gravel mineralogy								
		Shape	Rock type	Degree of alteration	Surface features	Gravel					IR ^c	Calcite ^d	Dolomite ^d	Fe ₂ O ₃ :CD ^e	TiO ₂ /mg kg ⁻¹	ZrO ₂ /mg kg ⁻¹	TiO ₂ /ZrO ₂	
						Total ^b	Coarse	Fine	Clay	Silt								Sand
P1	A	pl/sb	ls	wa	rd, ar	16	85	15	33.6	48.3	18.1	13	85	2	0.78	400	18	22
	Bt	ir/pl	ls/qz	wa	rd, car/ar	7	80	20	28.4	43.6	28.0	15	85	0	0.69	500	18	28
	2R	-	ls	tec	rd, car	-	-	-	45.8	52.8	1.4	21	79	0	ND	800	30	27
P2	Ah	pl/sb	do/ls	na	rd, ar	23	82	18	28.4	47.3	24.3	18	18	64	1.13	500	ND	ND
	Bt	sb/pl	do	a	ar	8	79	21	31.6	61.9	6.5	12	0	88	0.85	300	8	38
	R	-	do/ls	tec	rd, car/ar	-	-	-	33.7	56.2	10.1	1	16	83	ND	200	ND	ND
P3	A	sb/rd	clsbr	wa	car/ar	12	77	23	45.3	32.0	22.7	29	46	25	1.70	700	32	22
	2Bt	sb	clsbr	wa	car/ar	8	75	25	72.5	18.8	8.7	29	71	0	1.75	2400	68	35
	2R	-	clsbr	na	-	-	-	-	78.1	15.1	6.8	22	78	0	ND	1600	45	36
P4	Ah	pl/ag	ls	wa	rd, ar	18	90	10	40.6	45.1	14.3	16	84	0	1.91	400	17	25
	Bw	pl/sb	ls	wa	ar/car	11	98	2	39.2	47.6	13.2	17	83	tr	1.20	800	23	35
	C	pl	m/s	a	-	81	ND	ND	ND	ND	ND	ND	ND	ND	ND	200	ND	ND
	2R	-	clsbr	na	rd	ND	ND	ND	22.7	51.7	25.6	17	81	2	ND	400	ND	ND

^aShape: pl, plane; ag, angular; sb, subrounded; rd, rounded; ir, irregular. Rock type: ls, limestone; m/s, marly limestone; qz, quartzite; do, dolostone; clsbr, cemented limestone breccia. Degree of alteration: na, non-altered; wa, weakly altered; a, altered; tec, with cataclasis. Surface features: rd, dissolution marks; ar, clay coatings; car, carbonate coatings. ^bWhole soil.

^cIR, insoluble residue obtained by weighing.

^dXRD adjusted with proportions of IR:

$$\% \text{ calcite} = \frac{\% \text{ calcite XRD} \times (100 - \text{IR})}{\% \text{ calcite XRD} + \% \text{ dolomite XRD}}; \quad \% \text{ dolomite} = \frac{\% \text{ dolomite XRD} \times (100 - \text{IR})}{\% \text{ calcite XRD} + \% \text{ dolomite XRD}}; \quad \% \text{ IR} + \% \text{ calcite} + \% \text{ dolomite} = 100.$$

^eCD, citrate-dithionite.

ND, not determined.

proportions of insoluble residue were obtained by weighing the initial and final material. The clay, silt and sand proportions of the insoluble residue were determined and a fine fraction (<0.05 mm = silt + clay) and a sand fraction (>0.05 mm) were separated for later analysis.

Other properties analysed were as follows. The organic carbon content of the fine earth was determined by dichromate oxidation; the CaCO_3 equivalent in the fine earth by Bernard's calcimeter; the cation exchange capacity (CEC) and base saturation of the fine earth by the ammonium acetate (pH 7)–sodium chloride method; the pH in a 1:1 suspension of fine earth:water; forms of free iron oxide in the fine earth and insoluble residue by the sodium citrate–dithionite method and total iron in the fine earth by digestion in HF-HClO_4 ; and Fe in solution was measured by atomic absorption spectrometry. The Ti and Zr content in the fine earth, gravel and rock was determined by X-ray fluorescence with Philips PW 1404 equipment with a Dual XR Cr-Au, various analysing crystals on a sample of dust fused with $\text{Li}_2\text{B}_4\text{O}_7$ (Philips Perl'X-2 equipment) (1:10, weight/weight).

Solutions were obtained from saturation pastes of fine earth and in these were measured pH, Na^+ , K^+ (flame ionization photometry), Ca^{2+} , Mg^{2+} and SiO_2 (atomic absorption spectrometry).

X-ray diffraction (XRD) traces of samples of unoriented powder were obtained by using a holder filled from the side. Forms of free iron were previously removed from all the fine fractions (<0.05 mm) by the sodium citrate–dithionite extraction. The equipment and operating conditions were as follows: Philips PW 1730 diffractometer, radiation ($\text{Cu-K}\alpha$), 35 kV, 15 mA, scan speed $2^\circ 2\theta$ minute⁻¹, paper speed 2 cm per degree 2θ , time constant 2 s. Oriented aggregates of silt and clay fractions were prepared by sedimentation and drying on glass slides, and subjected to ethylene glycol and dimethylsulphoxide (DMSO) solvations, and thermal treatment (550°C) as described by Brown & Brindley (1980) and González-García & Sánchez-Camazano (1968). The quantitative analysis was determined using the intensity factors method (Delgado *et al.*, 1982). The proportions of non-carbonate mineral phases (XRD) in the gravels and rocks and the proportions estimated by weighing the insoluble residue were similar. This permitted us to calculate an adjusted mineral analysis of calcite and dolomite (Table 3).

Crystallochemical parameters of mica were determined by XRD (Martín-García *et al.*, 1997, 1998). The micaceous nature of the mineral was confirmed by the method of Srodon & Eberl (1984). The b_0 parameter was estimated from the 060 reflection (≈ 0.150 nm) in unoriented powder. The experimental conditions were: angular range 59 – $64^\circ 2\theta$, scan speed $0.2^\circ 2\theta$ minute⁻¹, paper speed 0.5 cm minute⁻¹, time constant 0.4 s. The illite crystallinity index (IC) was measured as described by Kisch (1991). Crystallite size was calculated using the Scherrer equation (Klug & Alexander, 1976); we used a pectatitic phengite from the Pedroches area (Córdoba) as a crystal size standard (>100 nm). The percentage of $2M_1$ polytypes ($\% 2M_1 = 100 \times 2M_1 / (1M + 2M_1)$) in unoriented powder was

determined according to Tettenhorst & Corbató (1993); quartz in the sample was used as an internal standard, and, when necessary, pure quartz was added.

Differential thermal analysis (DTA) and thermal gravimetric analysis (TG) were carried out with NETZSCH Simultaneous Thermal Analysis STA 409 EP equipment at a heating rate of 10°C minute⁻¹, with alumina sample holders, over a temperature range of 20 to 1010°C .

Coarse and fine sand, and silt particles in the fine earth and insoluble residue of horizons A and Bt of profiles P1 and P3 were observed by scanning electron microscope (SEM) (Hitachi S-510, acceleration voltage at 25 kV). The materials were mounted on two-sided adhesive paper, fixed to the sample holder with colloidal silver and metallized with gold deposited in two orientations (20–30°).

Results

Macromorphology and micromorphology

The soils are red and reddish with B horizons of hue 2.5YR (Table 2). Horizon Bw in P4 is classified as a Cambic horizon because, amongst other characteristics, it has a redder hue than the C horizon.

Visual analysis of the coarse fragments and rock substratum fragments, together with the mineralogical data obtained by XRD (Tables 1 and 3), shows the following.

- 1 The sedimentary rocks are mostly compact and calcareous containing some non-calcareous detrital material; they include limestone, marly limestone, dolomitic limestone, and cemented limestone breccia. Quartzite detritus occurs in one profile (P1); quartzites are present elsewhere in the stratigraphic sequence of the Alpujarride nappes to which the calcareous rocks belong.
- 2 There are lithological differences between the soil rock fragments and the underlying rocky substrate: marly limestones occur over cemented limestone breccia in P4; quartzite occurs over limestone in P1; the coarse fragments in the A horizon of P3 are more dolomitic than the underlying rock (Table 3). These differences in the parent material are indicated by the horizon notation (Table 2).
- 3 The effects of the carbonate dissolution and the various alteration processes can be seen on the surfaces of the gravel fragments as dissolution marks, dark reddish-brown secondary carbonate deposits, and clay patinas.

In the field study, cutans could be seen in the Bt horizons of profiles P1, P2 and P3; micromorphologically they are polycyclic illuviation cutans and occupied more than 1% of the sections and are thus Argic horizons according to FAO (1998) (Table 2).

Analytical characteristics

The fine earths of all the soils have a large content of silt or clay or both (Table 4). The greater clay contents of the Bt

Table 4 Selected properties of the fine earth

Profile	Horizon	Particle size distribution						OC	CaCO ₃ eq. /cmol _c kg ⁻¹	CEC /cmol _c kg ⁻¹	Base saturation /%	pH	Fe ₂ O ₃			Fe ₂ O ₃ -CD			TiO ₂ /mg kg ⁻¹	ZrO ₂ /mg kg ⁻¹	TiO ₂ /ZrO ₂	
		Clay	Silt	Coarse sand	Fine sand	OC	CaCO ₃ eq.						CD	Total	100 × CD/Total	fine earth/ Fe ₂ O ₃ -CD	IR ^a	Fe ₂ O ₃				ZrO ₂
		/%											/%	/%	/%	/%	/%	/%				/%
P1	A	17.4	61.4	4.5	16.7	3.3	1.7	21.5	100	8.0	5.43	8.04	68	7.0	10900	249	43.8					
	Bt	41.8	44.5	3.5	10.2	1.5	0.7	22.9	94	8.1	6.15	8.48	73	8.9	9900	221	44.8					
P2	Ah	27.2	53.0	5.9	13.9	2.6	2.4	22.3	100	8.1	5.29	7.81	68	4.7	10500	231	45.5					
	Bt	55.0	31.2	3.8	10.0	1.6	1.8	21.0	100	8.1	6.44	8.89	72	7.6	9000	183	49.2					
P3	A	22.2	38.9	6.3	32.6	0.9	20.2	19.9	100	8.2	4.43	8.10	55	2.6	9300	212	43.9					
	2Bt	48.4	36.5	2.5	12.6	1.0	0.8	22.1	100	8.3	6.86	7.24	95	3.9	9500	281	33.8					
P4	Ah	49.2	42.1	3.8	4.9	4.2	1.0	23.9	100	7.6	5.86	6.78	86	3.1	9300	265	35.1					
	Bw	47.9	43.0	4.2	4.9	1.0	1.0	16.7	100	8.1	6.58	8.26	80	5.5	9200	185	49.7					
	C	42.9	34.7	13.0	9.4	1.0	26.6	9.8	100	8.0	6.15	8.52	72	–	7000	152	46.1					

^aValues of Fe₂O₃ in the IR in Table 3.OC, organic carbon; CaCO₃ eq., calcium carbonate equivalent; CEC, cation exchange capacity; CD, citrate-dithionite; IR, insoluble residue.

Argic horizon of profiles P1, P2 and P3 are evidence for illuviation. The ratios (% clay A)/(% clay Bt) were 1/2.4, 1/2.0 and 1/2.3, respectively. However, this tendency was not present in P4 which has a Cambic horizon (ratio (% clay A)/(% clay B) = 1/1).

The gravel fraction of all horizons is less than 23% of the whole soil, except in the C horizon of P4, where it is 81% (Table 3). This gravel is mainly coarse (> 8 mm). The insoluble residue of the gravels and rocks ranges between 12 and 29%, except in the dolomitic limestone of P2 where it is 1% and in the gravel of the C horizon of P4 (73%). These relatively large values are consistent with the marly and brecciated nature of many of the materials and are similar to those found by Durn *et al.* (1999). The fine fractions (silt and clay) dominate the insoluble residue which is of varied silty clay loam, clay, clay loam, silty clay and silt loam textures.

Decalcification is nearly complete in the fine earth of the B horizons (Table 4). The Fe₂O₃-CD content of the fine earth ranges from 4.4 to 6.9% (mean 5.9%). The ratio (% Fe₂O₃-CD in horizon A)/(% Fe₂O₃-CD in horizon B) is 1/1.1, 1/1.2, 1/1.5 and 1/1.1 in P1, P2, P3 and P4, respectively. The greater contents in the B horizons can be attributed to alteration and/or illuviation of the iron oxides accompanying the clay. The Fe₂O₃-CD content of the insoluble residue (Table 3) is always less than 2% and always smaller than that of the corresponding fine earths. The insoluble residue from P4 has the largest Fe₂O₃-CD. This explains the large iron oxide content of the fine earth of this profile (Table 4) which cannot easily be attributed to the illuviation as it lacks a Bt horizon.

The ratio (% Fe₂O₃-CD in fine earth)/(% Fe₂O₃-CD in insoluble residue) is always greater than 1 (2.6–8.9) (Table 4), which indicates a process of alteration and concentration of iron oxides in the fine earth of the soil relative to the insoluble residue. In each profile the ratio is greater in Bt or Bw than in the A horizon. In the fine earth, the free iron oxides account for 55–95% (mean 74%) of total Fe (Table 4). The likely formation of Fe oxides is consistent with the rubification of the soil.

The TiO₂/ZrO₂ ratios (43.8–49.7) of the fine earths (Table 4) are similar in all the horizons analysed except in the Bt horizon of P3 and the Ah horizon of P4 (33.8 and 35.1, respectively). The TiO₂/ZrO₂ ratios in the gravels and rocks (Table 3) differ more and some could not be determined because the quantities of Zr present were too small. Generally, the values are smaller than those in the fine earth.

Mineralogical composition

Calcite and dolomite are abundant in the gravels and rocky substrata (Table 3), and are also present in the coarse and fine sand (Table 5). Quartz, feldspars and phyllosilicates (illite; K-mica; paragonite; Na-mica; kaolinite; chlorite; occasionally small amounts of smectite) are present in the insoluble residue, and in the sand, silt and clay fractions of the fine earth

(Table 5). The K-micas are the most abundant phyllosilicate. The free iron oxides are haematite and goethite.

The presence of kaolinite was established by XRD using DMSO treatments and was confirmed by thermal analysis of iron oxide free samples of clay and silt which gave an endothermic peak between 400 and 600°C.

The sands of the fine earth generally contain more phyllosilicates and iron oxides than the sands in their corresponding insoluble residues (Table 5). This suggests a more complex origin than simple dissolution and inheritance from the insoluble residue and is discussed in the SEM section below.

Crystallochemical parameters of mica

The micas did not have a significant proportion of expanding layers, since the reflection values (ethylene glycol) [002] were greater than 17.72°2θ and [003] less than 26.79°2θ, so they are micas *sensu stricto* rather than interstratified mica-smectite (Srodon & Eberl, 1984). This condition has to be met to use the methodology for the measurement of the crystallochemical parameters. The fact that the mica is not degraded shows that it has been derived from elsewhere. Also, since the mica is not degraded, the transformed phases of these soils such as the interstratified phases are scarce (Table 5).

The values of b_0 obtained (Table 6) ranged between 0.8998 nm and 0.9032 nm, corresponding to dioctahedral micas (Griffen, 1992). The value of b_0 of the unit cell is correlated in micas to the atomic compositions of the tetrahedral and octahedral sheets and interlaminar sites (Guidotti *et al.*, 1989). Using our values of b_0 in the equations of Martín-García *et al.* (1997) (calculated for micas of Andalusian red soils) we were able to estimate the average structural formulae of micas in the study (Table 7). The main limitations of such calculations are (i) the Fe present has to be assumed to be Fe³⁺ because it is difficult to distinguish Fe²⁺ and Fe³⁺ in white micas (Guidotti, 1984), and (ii) there is a possible error in the measurement of b_0 because of the 060 reflection of paragonite (Na-mica) or kaolinite, which are also dioctahedral. This error is small, however, since there is little paragonite, and kaolinite has a smaller 060 spacing so it should not contribute much to the error.

All micas (Table 7) have a tetrahedral sheet with greater silica and smaller aluminium contents than ideal muscovite, thus giving a tetrahedral charge less than 1 to this layer (x^{IV} between -0.72 and -0.89). The cation of the octahedral sheet is essentially Al³⁺ with some substitution of Mg²⁺ and Fe³⁺, implying a certain phengitic character and the presence of an octahedral charge (x^{VI}). This does not occur in the ideal muscovites (Table 7) where all the charge is tetrahedral. In the micas studied x^{VI} ranged between -0.04 and -0.16. The resulting layer charge ($x = x^{IV} + x^{VI}$) for a half-cell unit is close to -1.0 in the fine fractions of insoluble residue and

Table 5 Mineralogical analysis (XRD) of the clay, silt and insoluble residue (silt + clay and sand)

Profile	Horizon	Sand fractions ^a (2–0.05 mm) /%									Fine fractions ^b (<0.05 mm) /%							
		Fraction	Cal	Dol	Q	Phyll	Ox Fe	FdK	FdNa	Fraction	Q	FdK	FdNa	Ill	K	Pg	Chl	Sm
P1	A	CS	16	4	47	26	5	1	1	C	7	1	2	64	22	3	1	0
		FS	0	2	63	26	5	2	2	S	59	3	0	31	3	1	3	0
		SIR	0	0	97	2	0	1	0	IR	41	1	1	57	1	0	<1	0
	Bt	CS	10	0	58	25	5	1	1	C	11	3	1	65	18	1	1	0
		FS	0	0	69	25	3	0	3	S	50	3	0	37	7	2	1	tr
		SIR	0	0	95	2	0	2	1	IR	38	1	1	59	1	0	<1	0
2R	SIR	0	0	62	28	9	1	0	IR	26	1	0	73	tr	0	tr	0	
P2	Ah	CS	5	10	37	42	3	3	0	C	11	1	1	63	19	2	3	0
		FS	0	5	68	19	3	2	3	S	42	3	1	37	12	2	3	tr
		SIR	0	0	77	20	0	3	0	IR	46	1	0	48	3	1	1	0
	Bt	CS	3	13	55	28	0	1	0	C	7	1	0	61	24	3	4	0
		FS	0	12	60	22	2	2	2	S	44	5	1	35	8	3	4	0
	SIR	0	0	81	18	0	1	0	IR	51	2	0	45	2	0	0	0	
R	SIR	0	0	69	30	0	1	0	IR	ND	ND	ND	ND	ND	ND	ND	ND	
P3	A	CS	22	13	50	11	4	tr	0	C	8	1	0	66	20	3	2	0
		FS	5	12	60	16	3	0	4	S	54	3	0	32	6	3	2	0
		SIR	0	0	95	5	0	0	0	IR	43	1	0	46	7	0	3	0
	2Bt	CS	14	0	68	13	5	0	0	C	6	1	0	73	16	1	3	0
		FS	0	0	76	19	2	1	2	S	63	3	2	22	6	2	2	0
	SIR	0	0	87	13	0	0	0	IR	35	1	1	45	10	4	4	0	
2R	SIR	0	0	88	9	0	2	1	IR	14	1	0	55	21	0	5	4	
P4	Ah	CS	6	0	64	26	3	1	0	C	5	4	1	82	5	1	2	tr
		FS	0	0	53	38	4	1	4	S	61	2	2	27	6	0	1	1
		SIR	0	0	90	9	0	1	0	IR	39	1	1	53	3	0	3	0
	Bw	CS	4	2	47	39	6	1	1	C	5	4	tr	81	7	1	2	0
		FS	1	0	59	33	4	2	1	S	56	4	2	29	5	0	1	3
		SIR	0	0	72	26	0	1	1	IR	58	1	<1	36	3	0	2	0
	C	CS	ND	ND	ND	ND	ND	ND	ND	C	4	4	<1	86	6	0	<1	0
		FS	ND	ND	ND	ND	ND	ND	ND	S	41	2	0	52	3	0	1	1
	2R	SIR	0	0	81	17	1	1	0	IR	58	2	0	39	1	0	<1	0

^aCS, coarse sand (2–0.25 mm); FS, fine sand (0.25–0.05 mm); SIR, sand of insoluble residue (2–0.05 mm). Mineralogy: Cal, calcite; Dol, dolomite; Q, quartz; Phyll, phyllosilicates; Ox Fe, iron oxides (goethite and haematite); FdK, potassium feldspar; FdNa, sodium feldspar.

^bC, clay (<2 μm); S, silt (2–50 μm); IR, clay + silt of insoluble residue. Free iron forms were previously removed from these fractions for analysis. Mineralogy: Q, quartz; FdK, potassium feldspar; FdNa, sodium feldspar; Ill, illite; K, kaolinite; Pg, paragonite; Chl, chlorite; Sm, smectite. ND, not determined; tr, trace.

between –0.76 and –0.97 in the silt and clay fractions of fine earth. The micas in our *terrae rossae* can thus be classified as illites, mostly of a high charge (Velde, 1985) that is close to muscovite, and with a degree of phengitization.

The percentage of polytypes $2M_1$ ($\%2M_1 = 100 \times [2M_1 / (2M_1 + 1M)]$) and the crystallinity index of illite (IC) are shown in Table 6. The proportion of insoluble residue polytype is large ($\%2M_1$ 76–100, mean 88) and becomes much smaller in the silt ($\%2M_1$ 39–81, mean 56) and the clay fractions ($\%2M_1$ 11–31, mean 22). The illite crystallinity index of the micas increases from the insoluble residue to silt then clay; consequently the effective crystallite size of illite decreases from insoluble residue to clay; the illite crystallinity index is greatest in the clays of the B horizons.

SEM observations

In the sand fractions of the fine earth most of the grains are of a single mineral and varied morphology (Figure 3a). Nowhere did we find spherical carbonate particles, typical of bioliths of bacterial origin (Rivadeneira *et al.*, 1997). There were, however, some pseudospherical, subrounded, cemented particles (Figure 3b) in which single mineral grains are embedded in what could be a phyllosilicated matrix of the soil (Figure 3c). These are probably aggregated particles strongly cemented by iron oxides and resistant to breakdown in the laboratory. These observations explain the mineralogical composition of the sand of the fine earth, relatively rich in phyllosilicates and iron oxides. Aggregated particle groups also occur in the

Table 6 Crystallochemical parameters of micas

Profile/ Horizon	Fine earth																		
	Insoluble residue (silt + clay)						Silt			Clay									
	002 ^a °2θ	003 ^a °2θ	b ₀ /nm	2M ₁ /%	IC ^b	Crystallite size ^c /nm	002 °2θ	003 °2θ	b ₀ /nm	2M ₁ /%	IC ^b	Crystallite size ^c /nm							
P1	A	17.763	26.740	0.9001	100	0.43	65	17.747	26.677	0.9014	90	0.32	>100	17.755	26.747	0.9004	18	0.62	22
	Bt	17.763	26.732	0.9002	100	0.40	82	17.751	26.677	0.9007	50	0.41	74	17.750	26.707	0.9008	28	0.73	17
	2R	17.747	26.787	0.9006	26	ND	ND												
	Mean P1 ^d	17.758	26.751	0.9003	76			17.750	26.677	0.9009	60	0.39		17.751	26.717	0.9007	26	0.70	18
P2	Ah	17.763	26.704	0.9006	34	0.40	84	17.783	26.709	0.9009	31	0.41	74	17.757	26.761	0.9010	22	0.71	18
	Bt	17.724	26.692	0.8998	100	0.36	>100	17.779	26.669	0.9008	44	0.43	65	17.802	26.787	0.9008	19	0.79	14
	Mean P2 ^d	17.739	26.697	0.9001	75	0.38		17.781	26.684	0.9008	39	0.42	68	17.784	26.777	0.9009	20	0.76	16
P3	A	17.763	26.661	0.8999	100	0.42	68	17.771	26.677	0.9009	27	0.39	90	17.802	26.755	0.9022	10	0.71	18
	2Bt	17.755	26.700	0.9002	100	0.46	48	17.763	26.661	0.9014	52	0.38	>100	17.779	26.692	0.9032	12	ND	ND
	2R	17.747	26.724	0.8998	100	0.47	46												
	Mean P3 ^d	17.755	26.695	0.9000	100	0.45	53	17.766	26.667	0.9012	42	0.38		17.788	26.717	0.9028	11		
P4	Ah	17.724	26.740	0.9016	100	0.39	90	17.763	26.740	0.9019	62	0.41	74	17.771	26.755	0.9026	21	0.49	41
	Bw	17.763	26.740	0.9010	100	0.32	>100	17.795	26.732	0.9011	100	0.39	90	17.747	26.740	0.9026	37	0.59	25
	C	17.763	26.740	0.9011	100	0.39	90	17.755	26.787	0.9014	70	0.32	>100	17.755	26.747	0.9032	34	0.59	25
	Mean P4 ^d	17.751	26.740	0.9012	100	0.36		17.776	26.748	0.9014	81	0.38		17.756	26.746	0.9027	31	0.56	29
Total mean		17.751	26.721	0.9004	88			17.768	26.694	0.9011	56	0.39		17.770	26.739	0.9018	22		
σ _{n-1}		0.008	0.029	0.0005	14			0.014	0.037	0.0003	19	0.02		0.019	0.029	0.0011	9		

^aPeak position for glycol-treated samples.^bIC, illite crystallinity (half-peak width of the 1.0 nm mica peak in oriented preparations).^cPerpendicular to [00c] planes.^dProfile means weighted to horizon thickness.

ND, not determined.

Table 7 Crystallochemical parameters of the structural formulae of the micas (mean values for half-cell unit)

		Structural formulae				
		Tetrahedral sheet	Octahedral sheet ^a	x^{IV}	x^{VI}	x
P1	Insoluble residue	(Si _{3.13} Al _{0.87})	Al _{1.77} (Fe,Mg) _{0.22}	-0.87	-0.14	-1.02
	Silt (fine earth)	(Si _{3.16} Al _{0.84})	Al _{1.75} (Fe,Mg) _{0.25}	-0.84	-0.13	-0.95
	Clay (fine earth)	(Si _{3.15} Al _{0.85})	Al _{1.76} (Fe,Mg) _{0.24}	-0.85	-0.13	-0.97
P2	Insoluble residue	(Si _{3.12} Al _{0.88})	Al _{1.78} (Fe,Mg) _{0.21}	-0.88	-0.15	-1.04
	Silt (fine earth)	(Si _{3.16} Al _{0.84})	Al _{1.76} (Fe,Mg) _{0.24}	-0.84	-0.12	-0.96
	Clay (fine earth)	(Si _{3.16} Al _{0.84})	Al _{1.75} (Fe,Mg) _{0.25}	-0.84	-0.12	-0.95
P3	Insoluble residue	(Si _{3.11} Al _{0.89})	Al _{1.78} (Fe,Mg) _{0.20}	-0.89	-0.16	-1.05
	Silt (fine earth)	(Si _{3.18} Al _{0.82})	Al _{1.74} (Fe,Mg) _{0.26}	-0.82	-0.11	-0.92
	Clay (fine earth)	(Si _{3.28} Al _{0.72})	Al _{1.70} (Fe,Mg) _{0.35}	-0.72	-0.04	-0.76
P4	Insoluble residue	(Si _{3.18} Al _{0.82})	Al _{1.74} (Fe,Mg) _{0.26}	-0.82	-0.11	-0.92
	Silt (fine earth)	(Si _{3.20} Al _{0.80})	Al _{1.74} (Fe,Mg) _{0.27}	-0.80	-0.10	-0.90
	Clay (fine earth)	(Si _{3.27} Al _{0.73})	Al _{1.70} (Fe,Mg) _{0.34}	-0.73	-0.05	-0.77
Mean	Insoluble residue	(Si _{3.13} Al _{0.87})	Al _{1.77} (Fe,Mg) _{0.22}	-0.87	-0.14	-1.01
	Silt (fine earth)	(Si _{3.18} Al _{0.82})	Al _{1.75} (Fe,Mg) _{0.26}	-0.82	-0.11	-0.93
	Clay (fine earth)	(Si _{3.22} Al _{0.78})	Al _{1.73} (Fe,Mg) _{0.29}	-0.78	-0.08	-0.86

^aFe as Fe³⁺ (Guidotti, 1984).

The formulae are calculated from the values of b_0 (mean values, Table 6) using the equations of Martín-García *et al.* (1997).

x^{IV} , tetrahedral charge; x^{VI} , octahedral charge; x , layer charge.

Formula of ideal muscovite: (Si₃Al)Al₂O₁₀(OH)₂K; $x^{IV} = -1$; $x^{VI} = 0$; $x = -1$.

silt fraction (Figure 3d), but here have a more cemented appearance.

In our SEM studies of quartz grains from both sand and silt fractions we found they had very varied morphologies, as follows.

1 Quartz grains occur as fresh, irregular, angular fragments, with no sign of polyhedral faces. The grains have clean surfaces, marked edges, or typical concoid fractures with parallel and arcuate steps (Figure 3a). Similar grains to these occur in the insoluble residue (Figure 3e).

2 Quartz grains also occur as idiomorphic crystals (euhedral), or almost so, with polyhedral faces showing features related to crystalline growth (Figure 3f). Some of these grains have a superficial fine granular film, possibly of colloidal silica (Figure 3g).

3 We also found a wide range of other quartz morphologies, the common characteristics of which are to be physically weathered and to show various effects of mechanical action such as a smooth surface, or various types of surface breakage or dissolution features such as V-shaped pits, grooves, striations, steps, and irregular surfaces due to fractures and holes. These morphologies include (i) hypidiomorphic (subeuhedral) grains, reminiscent of a polyhedron (Figure 3h), (ii) irregular detrital fragments (Figure 3i), and (iii) elongated, evolved quartzite grains (Figure 3j). The presence of these grains provides further evidence of complex soil development because physical weathering does not occur in the stable soil environment of the *terrae rossae*.

We also used SEM to look at the phyllosilicated fractions in our soils. We found aggregated forms of the phyllosilicates in the sand fraction of the insoluble residue (Figure 3k). These were composed of layers < 20 μm thick with some degree of continuity between the layers which were partially cemented together (Figure 3e). We believe that these are of sedimentary origin and that they disintegrate in the soil environment to give phyllosilicate particles. In the fine silt fraction of the fine earth we found phyllosilicated particles which resembled single crystals, some of which had a few layers showing evidence of surface growth in the form of steps and edges with angles of 120° (Figure 3l). Such features are typical of kaolinite grains that have grown further.

Mineral phases in equilibrium with the soil solution

Solution compositions (Table 8) are plotted in the SiO₂-Al₂O₃-K₂O-H₂O equilibrium diagram (Garrels, 1984) (Figure 4). The points are within the fields of stability of kaolinite and close to those of montmorillonite.

Discussion

Autochthony versus allochthony of the soil material

The genetic relationship between the soil material (fine earth and coarse fragments) and the rocky substrate, whether autochthonous or allochthonous, can be assessed considering the following.

1 The relatively large contents of insoluble residue in our materials (12–29%, in Table 3) would seem to support an autochthonous origin.

2 There are lithological differences (lithological discontinuities) between the coarse fragments and the underlying rocky substrate as shown by direct observation and study of the mineralogical composition (Tables 1 and 3). This apparent allochthony must arise from colluvial movement of coarse fragments from upslope.

3 We calculated a clay balance as the percentage difference (Tables 3 and 4) between the percentage of the clay of the fine earth and that of the insoluble residue of its related gravel or underlying rocky substrate ($\Delta\text{clay} = \% \text{ clay in fine earth} - \% \text{ clay in IR}$) (Figure 5). When considering an autochthonous origin one should expect positive values for Δclay , since the fine earth should be richer in clay than the insoluble residue, due to the alteration processes undergone during dissolution of the rock. The clay balance should be greater in the Bt horizons due to clay illuviation. However, P1 and P3 generally have negative values of Δclay . In the context of autochthony, this would imply that clay has been lost from the fine earth, due to alteration, dissolution and clay movement (eluviation) and differential erosion. Another possible explanation is that the fine earth and/or the coarse fragments are allochthonous and derived from upslope, or, in the case of the fine earth, of wind-blown origin (Yaalon, 1997). This is not so for Δclay from the gravel and the rock in P2, nor for the Δclay from the gravel in P1. The values for these indicate selective enrichment of clay in the Bt horizons due to alteration and illuviation. Soil P4, with a Bw horizon, has positive differences in percentage clay throughout due to alteration of the minerals of the insoluble residue *in situ*.

If the profiles were truly homogeneous lithologically, one would expect Δclay for the insoluble residue of the rock to be greater than Δclay for the insoluble residue of the gravels, since, as shown morphologically (Table 3), the gravel is altered as demonstrated by Ugolini *et al.* (1996). Consequently, the gravel must contain altered mineral phases which would make their insoluble residue more clayey than that of their corresponding rock. This occurs only in P4. In P1, P3 and, to a lesser extent, in P2, the insoluble residue of the rock has more clay than the insoluble residue of the gravel so the Δclay is smallest in the insoluble residue of the rocks. Again, this suggests an allochthonous origin for the gravel.

4 The common presence, both in the soil fractions and in the insoluble residue, of quartz, sodium feldspar, potassium feldspar and the same mineral species of phyllosilicates (Table 5) can be considered as initial evidence for autochthony since these minerals would be released as insoluble residue from the rocks and stones as a result of their dissolution. In mineralogical terms this is a process of mineral inheritance. The principal species of phyllosilicates inherited would be illite (K-mica), paragonite (Na-mica) and chlorite, since kaolinite has a complex origin, as discussed below.

5 The ratio sum of inherited phyllosilicates (illite + paragonite + chlorite) divided by the sum of tectosilicates (quartz + sodium feldspar + potassium feldspar) ($\Sigma\text{IP}/\Sigma\text{T}$) was calculated for fine earths and insoluble residues to provide clues to mineral genesis. These are the most abundant mineral phases (Figure 6). The sums were obtained from the weighted means calculated from mineralogical analysis values of the three granulometric fractions (sand, silt + clay) (Tables 3–5). In the fine earth, the $\Sigma\text{IP}/\Sigma\text{T}$ values increase from Ah to Bt in all cases. This can be attributed principally to clay illuviation in the Bt. In the case of the insoluble residue, there are differences in P1, P3 and P4, between that from the coarse fragments of the various horizons and that from the underlying rock. When the values of $\Sigma\text{IP}/\Sigma\text{T}$ s for the fine earth are compared with their corresponding gravels they appear different, except in P3. Once again, differences in lithology and the allochthonous source of the materials are evident.

6 The ratios of $\text{TiO}_2/\text{ZrO}_2$ for the fine earths (Table 4) all have similar values, showing that they are relatively homogeneous in their chemical mineralogy. The ratios for the gravels (Table 3) vary more both between profiles and between horizons and the rocky substrate, which would support allochthony. This supports an allochthonous origin.

The source of quartz

The SEM study of quartz sand grains also provides new clues about the origin of the soil material. The various kinds of quartz grains shown in Figure 3 (SEM images) suggest they have varied origins. Some may come from the insoluble residue. The presence of angular, irregular, freshly broken detrital grains both in the fine earth (Figure 3a) and in the insoluble residue (Figure 3e) suggests inheritance from the gravel or bedrock as it is dissolved.

The morphology of the idiomorphic crystals (euhedral) (Figure 3f) with a superficial fine granular film, possibly of colloidal silica (Figure 3g), may be due to further crystal growth in the soil as described by Flageollet (1981) in African Ferralsols and Plinthosols and Torcal-Sáinz & Tello-Ripa (1992) in Spanish Planosols.

Some of the quartz grains are of wind-blown origin as is evident by their shape and size (Figure 3h–j), but the exact source of such grains is not known: they may come from more than one place. Particles similar to that in Figure 3(j) are easily blown about. They have a favourable aerodynamic shape with a smooth surface, like orange-peel with small holes, caused by wind abrasion under desert conditions (Folk, 1978). Other grains like those in Figure 3(h,i) have a smoother surface polish and oriented surface features suggesting a coastal origin (Margolis & Krinsley, 1974).

We suppose that airborne dust from the desertic or sub-desertic and coastal regions of either the African or the Spanish Mediterranean has contributed to the soil. Sierra Gádor is only 200 km from the North African coast and nearby deserts.

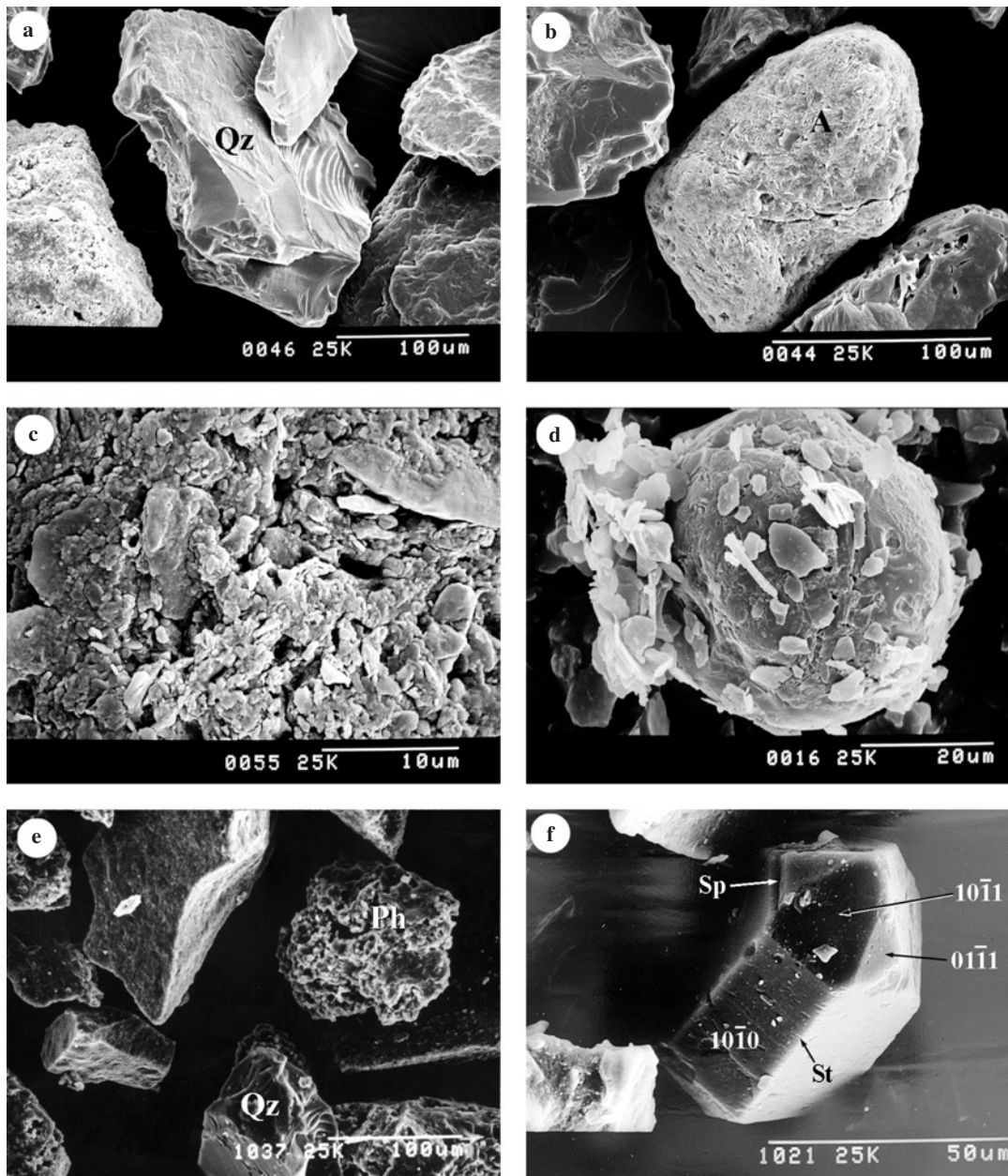


Figure 3 SEM photographs of selected particles. (a) Fine sand from the horizon A of P1. The quartz grain (Qz) in the centre is only slightly weathered. (b) Coarse sand from the Bt horizon of P3. The subrounded grain in the centre (A) is formed from aggregate particles. (c) Fine sand from the A horizon of P1, showing the detail of the surface of a group of particles similar to that in b. The porous skeletal laminar fabric is somewhat cemented and most grains are of fine silt and clay size ($< 20 \mu\text{m}$) with some of coarse silt size ($20\text{--}50 \mu\text{m}$). (d) Silt from the A horizon of P1. Pseudospherical aggregated particle with secondary cementation. (e) Sand from the insoluble residue of the gravel of the Bt horizon of P3. A quartz grain (Qz, bottom centre) with a characteristic concoidal fracture can be seen. Above, to the right, there is a cemented floccule of phyllosilicate laminae (Ph). (f) Fine sand grain from the A horizon of P1. This idiomorphic quartz crystal shows a hexagonal prism $[10\bar{1}0]$ and rhombohedral faces $[01\bar{1}1]$ forming a hexagonal pseudopyramid. The prism faces are striated (St) and there is a step (Sp) between these and those of the rhombohedron, thus duplicating the prism faces. (g) Fine sand from the A horizon of P1. Quartz grain showing polyhedral faces and fractured zones, coated with a fine granular layer of silica. (h) Fine sand from A horizon of P1. Subrounded hypidiomorphic quartz grain. There is a vacuole (V) in the left part of the grain. (i) Silt from the Bt horizon of P3. Irregular subrounded quartz grain with a polished surface and worn edges. Shows impact holes (h) and parallel lines and steps (Sp). (j) Fine sand from the A horizon of P1. Grain of aerodynamic form. (k) Sand-sized aggregate from the insoluble residue of the gravel from the Bt horizon of P3 formed from flocculated layers of phyllosilicate. (l) Silt from the Bt horizon of P3. Phyllosilicate crystal (of fine silt size) with hemihexagonal shape and angles of 120° between edges. Growth steps (Sp) and groups of small adhered laminae can be seen on the crystal surface.

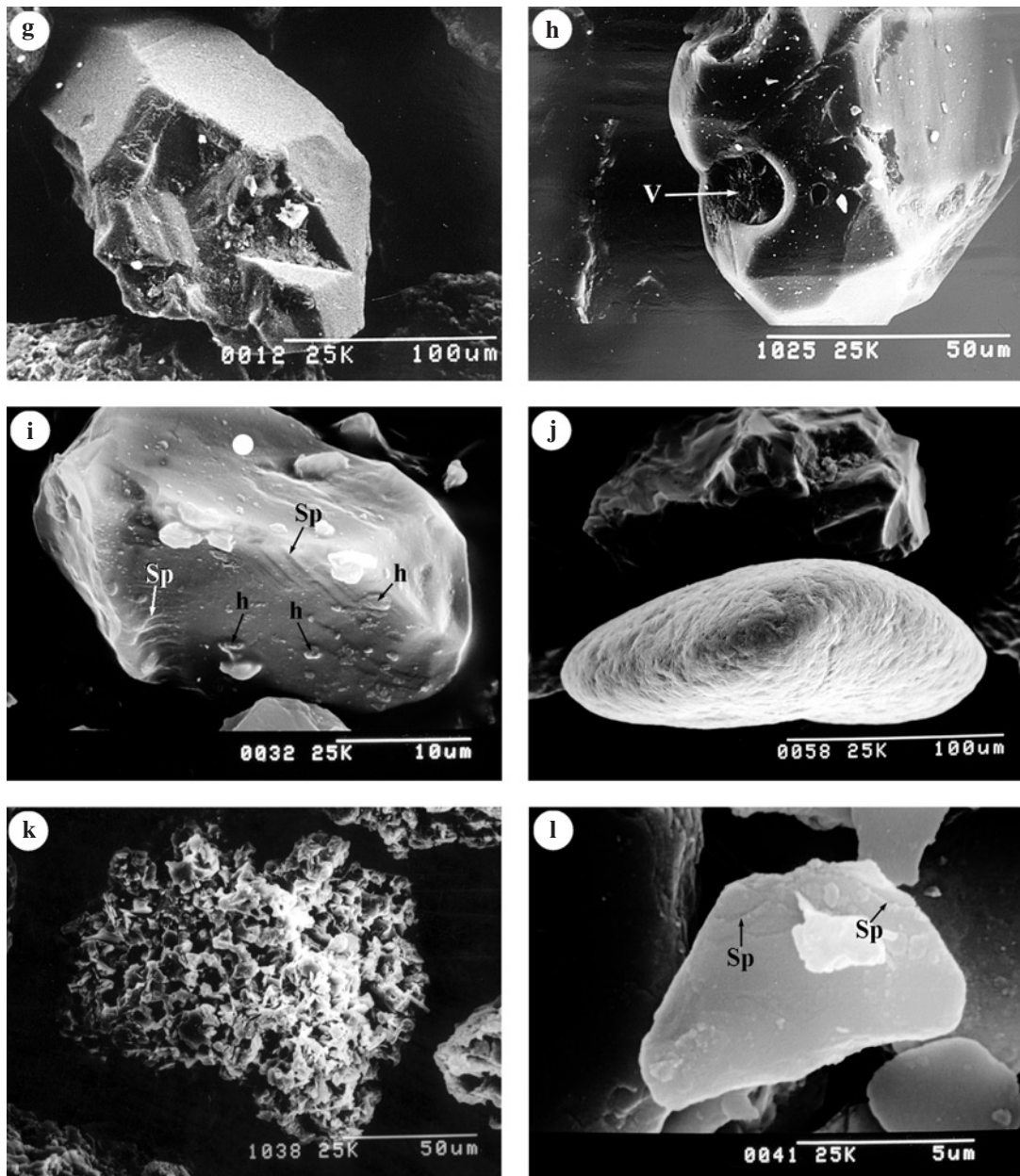


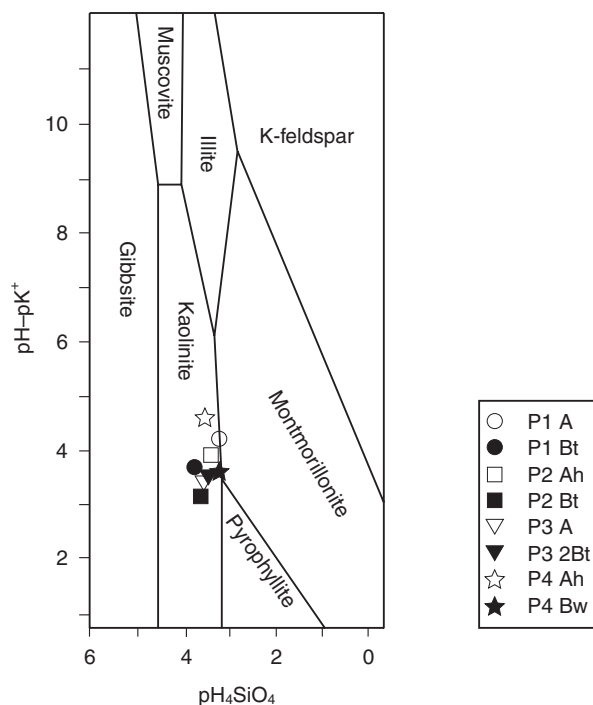
Figure 3 Continued

It is also within 25 km of the beaches of Almería and the subdesertic zones of southeast Spain. Thus, it is possible that the strong southerly winds could transport particles from these places. On the other hand, Ávila *et al.* (1997) found quartz in aeolian dust blown to Spain from the Sahara. Finally, Yaalon (1987) and Simonson (1995) relate the size of the grains and the distance they are transported. Very fine sand and coarse silt (20–100 μm) can cover moderate distances (50–200 km) and grains like those in Figure 3(h,i) are of this size. Such

grains are of coastal origin. Some of the grains have holes reminiscent of volcanic vacuoles (Figure 3h). These grains could have come from an extensive volcanic zone on the Almerian coast less than 50 km away. Particles larger than 100 μm can cover only short distances, by saltation. Particles of this size such as that in Figure 3(j) (75–200 μm) are therefore too large to have come from very far; however, they show an aeolian morphology and favourable aerodynamic shape. Their source is a mystery.

Table 8 Soil solution analysis (saturation extract)

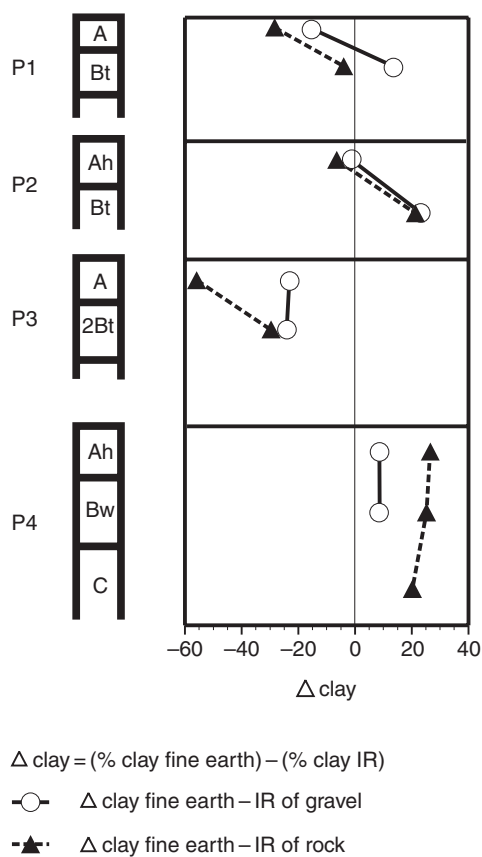
Profile	Horizon	pH	Na ⁺	K ⁺	Ca ²⁺	Mg ²⁺	Si ⁴⁺
			/mmol l ⁻¹				
P1	A	7.86	0.05	0.18	0.65	0.09	0.56
	Bt	7.69	0.13	0.15	0.99	0.07	0.16
P2	Ah	7.78	0.19	0.15	1.15	0.58	0.48
	Bt	7.65	0.07	0.08	0.57	0.05	0.20
P3	A	7.75	0.14	0.10	1.68	0.11	0.22
	2Bt	7.68	0.12	0.12	0.46	0.22	0.27
P4	Ah	8.07	0.13	0.24	1.10	0.34	0.35
	Bw	7.48	0.16	0.20	0.92	0.13	0.51
	C	7.92	0.13	0.08	0.68	0.11	0.09

**Figure 4** Stability relations of soil solutions and some mineral phases (25°C, 1 atm) in the SiO₂-Al₂O₃-K₂O-H₂O system as a function of pH-pK⁺ against pH₄SiO₄ (adapted from Garrels, 1984).

The SEM study thus confirms that the soil material of the *terrae rossae* contains quartz grains of both allochthonous and autochthonous origins.

The source of mica

The principal source of micas in the fine earth is by inheritance. This is supported by the fact that (i) the micas are

**Figure 5** Clay balance between fine earth and insoluble residue (IR).

present both in insoluble residue and in soil, (ii) they are found in large quantities (Table 5), and (iii) there are no significant quantities of interstratified swelling layers in the mica (reflection values [002] and [003] in Table 6; Srodon & Eberl, 1984), which would indicate a degradation process.

Comparison of the illites in the clay, silt, and silt + clay of the insoluble residue from a crystallochemical viewpoint (Table 7) warrants attention. Layer charge (x) decreases from insoluble residue to clay, due to the increase both in Si^{IV} and in the degree of phengitization (Fe + Mg)^{VI}. This is evidence for pedogenetic evolution or alteration (Fanning *et al.*, 1989). However, the differences between the micas in the insoluble residues and the mica in the soil clays of each profile are small and do not indicate significant differences in the mineral species; in all cases these are illites with large charge, similar to muscovite with some degree of phengitization. These results thus support the inheritance hypothesis known to be common to some degree to other red Mediterranean soils (Martín-García *et al.*, 1998). In P3 and P4 (Table 7), the differences between the micas in the clay fraction and those in the insoluble residue are greater than in P1 and P2, suggesting external, probably wind-blown, contributions. Unfortunately, there is no crystallochemical data available for the micas of Sahara dust to help verify this. Evidence for the aeolian

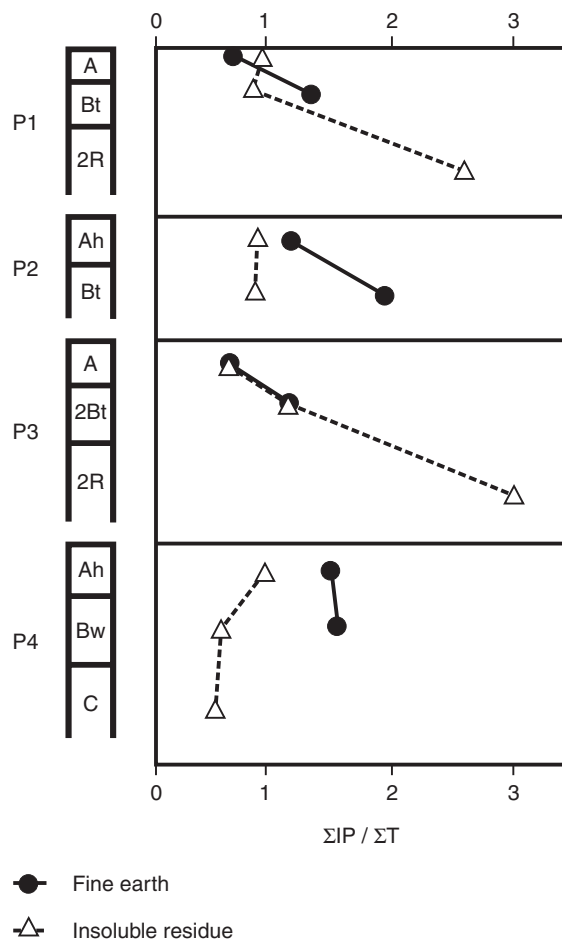


Figure 6 Ratio of Σ inherited phyllosilicates (IP)/ Σ tectosilicates (T). Inherited phyllosilicates: illite, paragonite and chlorite; tectosilicates: quartz, sodium feldspar and potassium feldspar.

contribution of micas to the soil is found in the mineralogical results for the atmospheric Saharan dust containing mica collected in Spain (Ávila *et al.*, 1997).

Comparison of percentage of polytypes $2M_1$ and the crystallinity index of illite of insoluble residues with the fine earth (Table 6) provides further information on the inheritance process. The percentage of polytypes $2M_1$ (with respect to $1M$) decreases from the insoluble residue (total mean 88%), via silt (56%), to the clay (22%), in agreement with the fact that $1M$ is a polytype of mica more typical of a low energy environment (Kisch, 1983) such as soil and that the granulometric fraction most adapted to the soil medium is the clay. Also, the ordered crystal size, as measured by the c axis, decreases from the insoluble residue to the clay as a direct result of the pedogenesis which decreases the size of the primary crystals. The clay fraction micas with the smallest crystal size are those for the B horizons since these horizons are the most reactive.

The position of the points representing the soil solution (Table 8) in the $\text{SiO}_2\text{-Al}_2\text{O}_3\text{-K}_2\text{O-H}_2\text{O}$ diagram (Figure 4),

outside the field of the potassium micas, indicates that these micas are unstable. The likely instability of the micas, together with their comparative abundance in the soil, once again suggests that they are inherited.

The results in Figure 4 are for the soil saturation extract, and it is possible to make an approximate extrapolation to a different moisture content of the soil *in situ*. Under the typical Mediterranean soil climate of these profiles (Figure 2) there is a wet season when the soil moisture can be assumed to match the conditions of the soil solution extract. In such wet periods the mica will be unstable (as shown in Figure 4), leading to crystal dissolution and migration of solutes. When the soil dries in summer (Figure 2) the solutions become more concentrated. This favours mica inheritance and helps to configure and stabilize the crystal-chemical modifications within the mica layer initiated in wet periods. The change in chemical behaviour of soil solutions with seasonal climate has been shown by Karatanasis (1991).

The source of kaolinite

The kaolinite of the fine earth, mainly present in the clay and silt fractions (Table 5), has two possible origins: inheritance and neoformation. The kaolinite could be inherited through dissolution of the rock. This process is supported by the mineralogical composition of the insoluble residue, which has significant quantities of this mineral. Another possible source of inheritance is the wind-blown dust which commonly contains kaolinites.

The kaolinite could also result from neoformation in the geochemical medium of the *terrae rossae*, as shown by the following.

1 Mineralogical composition: it is present in greater concentrations in the most reactive fraction, clay, than in the silt fraction or in the insoluble residue even when the decrease in the phyllosilicate content of the latter fractions is taken into account (Table 5).

2 Equilibria in the soil solution: the points are within the fields of stability of kaolinite (Figure 4); this is consistent with the idea that kaolinite is the stable mineral phase in Mediterranean soils where the activities of silica are slight (Torrent, 1995).

3 Morphological evidence by SEM: evidence of surface growth (steps and edges with angles of 120° , Figure 3l) are typical of kaolinite grains that have grown further.

Conclusion

From our results (analytical, textural, mineralogical, crystal-chemical, insoluble residue, geochemical and morphological using SEM) we conclude that the *terrae rossae* studied have both autochthonous materials, resulting from the dissolution of the underlying rocky substrate, and allochthonous ones that are the result of various processes, mainly colluviation from upslope and the accumulation of wind-blown particles.

Acknowledgements

This study was partly supported by project no PB98 1361.0 from the Spanish Ministry of Science and Technology. We thank Dr F.J. Huertas (CSIC, Granada) for the DTA and TG of some of the samples selected. We also thank Professor J. Torrent and Professor D.H. Yaalon and an anonymous reviewer for their constructive criticism of the script and their valuable suggestions. This paper is dedicated to Dr Gerardo Sánchez-Barrionuevo (1964–2000) who died suddenly at the start of our study.

References

- Ávila, A., Queralt-Mitjans, I. & Alarcón, M. 1997. Mineralogical composition of African dust delivered by red rains over northeastern Spain. *Journal of Geophysical Research*, **102**, 21977–21996.
- Bronger, A. & Bruhn-Lobin, N. 1997. Paleopedology of Terraes rossae–Rhodoxerals from Quaternary calcarenites in NW Morocco. *Catena*, **28**, 279–295.
- Brown, G. & Brindley, G.W. 1980. X-ray diffraction procedures for clay mineral identification. In: *Crystal Structures of Clay Minerals and X-ray Identification* (eds G.W. Brindley & G. Brown), pp. 305–359. Monograph No 5, Mineralogical Society, London.
- Delgado, R., Barahona, E., Huertas, F. & Linares, J. 1982. Los Mollisoles de la cuenca alta del río Dilar (Sierra Nevada). *Anales de Edafología y Agrobiología*, **41**, 59–82.
- Durn, G., Ottner, F. & Slovenec, D. 1999. Mineralogical and geochemical indicators of the polygenetic nature of terra rossa in Istria, Croatia. *Geoderma*, **91**, 125–150.
- Fanning, D.S., Keramidas, V.Z. & El-Desoky, M.A. 1989. Micas. In: *Minerals in Soil Environments* (eds J.B. Dixon & S.B. Weed), pp. 551–634. Soil Science Society of America, Madison, WI.
- FAO 1998. *World Reference Base for Soil Resources*. World Soil Resources Report 84, FAO, Rome.
- Flageollet, J.C. 1981. Aspects morphoscopiques et exoscopiques des quartz dans quelques sols ferrallitiques de la région de Cechi (Côte d'Ivoire). *Cahiers ORSTOM, Série Pédologique*, **18**, 111–121.
- Folk, R.L. 1978. Angularity and silica coatings of Simpson desert sand grains, Northern Territory, Australia. *Journal of Sedimentary Petrology*, **48**, 611–624.
- Garrels, R.M. 1984. Montmorillonite/illite stability diagrams. *Clays and Clay Minerals*, **32**, 161–166.
- González-García, S. & Sánchez-Camazano, M. 1968. Differentiation of kaolinite from chlorite by treatment with dimethylsulphoxide. *Clay Minerals*, **7**, 446–451.
- Griffen, D.T. 1992. *Silicate Crystal Chemistry*. Oxford University Press, New York.
- Guidotti, C.V. 1984. Micas in metamorphic rocks. In: *Micas* (ed. S.W. Bailey), pp. 357–467. Reviews of Mineralogy 13, Mineralogical Society of America, Washington, DC.
- Guidotti, C.V., Sassi, F.P. & Blencoe, J.G. 1989. Compositional controls on the *a*-cell and *b*-cell dimensions of $2M_1$ muscovite. *European Journal of Mineralogy*, **1**, 71–84.
- Karatanasis, A.D. 1991. Seasonal variation in solution composition and mineral stability of two Kentucky Alfisols. *Soil Science Society of America Journal*, **55**, 881–890.
- Kisch, H.J. 1983. Mineralogy and petrology of burial diagenesis (burial metamorphism) and incipient metamorphism in clastic rocks. In: *Developments in Sedimentology 25B: Diagenesis in Sediments and Sedimentary Rocks 2* (eds G. Larsen & G.V. Chilingar), pp. 289–493. Elsevier, Amsterdam.
- Kisch, H.J. 1991. Illite crystallinity: recommendations on sample preparation, X-ray diffraction settings, and interlaboratory samples. *Journal of Metamorphic Geology*, **9**, 665–670.
- Klug, H.P. & Alexander, L.E.C. 1976. *X-ray Diffraction Procedures for Polycrystalline and Amorphous Materials*. John Wiley & Sons, New York.
- Margolis, S.V. & Krinsley, D.H. 1974. Processes of formation and environmental occurrence of microfeatures on detrital quartz grains. *American Journal of Science*, **274**, 449–464.
- Martín-García, J.M., Delgado, G., Sánchez-Marañón, M., Párraga, J.F. & Delgado, R. 1997. Nature of dioctahedral micas in Spanish red soils. *Clay Minerals*, **32**, 107–121.
- Martín-García, J.M., Delgado, G., Párraga, J.F., Bech, J. & Delgado, R. 1998. Mineral formation in micaceous Mediterranean Red soils of Sierra Nevada, Granada, Spain. *European Journal of Soil Science*, **49**, 253–268.
- Moresi, M. & Mongelli, G. 1988. The relation between the terra rossa and the carbonate-free residue of the underlying limestones and dolostones in Apulia, Italy. *Clay Minerals*, **23**, 439–446.
- Olson, C.G., Ruhe, R.V. & Mausbach, M.J. 1980. Terra rossa limestone contact phenomena in Karst, Southern Indiana. *Soil Science Society of America Journal*, **44**, 1075–1079.
- Rivadeneira, M.A., Delgado, G., Ramos-Cormenzana, A. & Delgado, R. 1997. Precipitation of carbonates by *Deleya halophila* in liquid media: pedological implications in saline soils. *Arid Soil Research and Rehabilitation*, **11**, 35–47.
- Simonson, R.W. 1995. Airborne dust and its significance to soils. *Geoderma*, **65**, 1–43.
- Soil Survey Staff 1999. *Keys to Soil Taxonomy*, 8th edn. Soil Conservation Service/USDA/Pocahontas Press, Blacksburg, VA.
- Srodon, J. & Eberl, D.D. 1984. Illite. In: *Micas* (ed. S.W. Bailey), pp. 495–544. Reviews of Mineralogy 13, Mineralogical Society of America, Washington, DC.
- Tettenhorst, R.T. & Corbató, C.E. 1993. Quantitative analysis of mixtures of $1M$ and $2M_1$ dioctahedral micas by X-ray diffraction. *Clays and Clay Minerals*, **41**, 45–55.
- Torcal-Sáinz, L. & Tello-Ripa, B. 1992. *Análisis de sedimentos con microscopio electrónico de barrido: exoscopia del cuarzo y sus aplicaciones a la Geomorfología*. Cuadernos Técnicos de la Sociedad Española de Geomorfología No 4, Geofoma Ediciones, Logroño, Spain.
- Torrent, J. 1995. *Genesis and Properties of the Soils of the Mediterranean Regions*. Pubblicazione Università degli studi di Napoli, Federico II, Napoli.
- Torrent, J., Schwertmann, U., Fechter, H. & Alférez, F. 1983. Quantitative relationships between soil color and hematite content. *Soil Science*, **136**, 354–358.
- Ugolini, F.C., Corti, G., Agnelli, A. & Piccardi, F. 1996. Mineralogical, physical, and chemical properties of rock fragments in soil. *Soil Science*, **161**, 521–542.
- Velde, B. 1985. *Clay Minerals: A Physico-chemical Explanation of their Occurrence*. Developments in Sedimentology 40, Elsevier, Amsterdam.
- Yaalon, D.H. 1987. Saharan dust and desert loess: effect on surrounding soils. *Journal of African Earth Sciences*, **6**, 569–571.
- Yaalon, D.H. 1997. Soils in the Mediterranean region: what makes them different? *Catena*, **28**, 157–169.